European Drag Reduction and Flow Control Meeting – EDRFCM 2019
March 26–29 2019, Bad Herrenalb, Germany

SKIN-FRICTION DRAG REDUCTION DESCRIBED VIA THE ANISOTROPIC GENERALISED KOLMOGOROV EQUATIONS

A. Chiarini & M. Quadrio
Department of Aerospace Sciences and Technologies, Politecnico di Milano, via La Masa 34, 20156 Milano, Italy

D. Gatti
Institute of Fluid Mechanics, Karlsruhe Institute of Technology, 76131 Karlsruhe, Germany

In the present work, the recently introduced [1] Anisotropic Generalised Kolmogorov Equations, or AGKE, are used to investigate how skin-friction drag reduction alters the inter-component and multiscale processes of turbulence.

The AGKE are budget equations for the second-order structure function tensor $\langle \delta u_i \delta u_j \rangle$, where δu_i is the increment of the i-th velocity component at position $\boldsymbol{X}$ and separation $\boldsymbol{r}$, i.e. $\delta u_i = u_i(\boldsymbol{X}+\boldsymbol{r}/2) - u_i(\boldsymbol{X}-\boldsymbol{r}/2)$. In the general case, $\langle \delta u_i \delta u_j \rangle$ depends upon time and six independent spatial variables, i.e. the six coordinates of $\boldsymbol{X}$ and $\boldsymbol{r}$; they reduce to four in the indefinite plane channel geometry. The AGKE read:

$$\frac{\partial \langle \delta u_i \delta u_j \rangle}{\partial t} + \frac{\partial \phi_{k,ij}}{\partial r_k} + \frac{\partial \psi_{k,ij}}{\partial X_k} = P_{ij} + \Pi_{ij} + D_{ij} \qquad (1)$$

where $\boldsymbol{\phi}_{ij}$ and $\boldsymbol{\psi}_{ij}$ are fluxes of $\langle \delta u_i \delta u_j \rangle$ along directions of statistical inhomogeneity and among scales respectively, and P_{ij}, Π_{ij} and D_{ij} denote the production, pressure strain and viscous dissipation. Overall, the AGKE describe the production, transport and dissipation of the components of the scale Reynolds stresses in the combined physical ($\boldsymbol{X}$) and scale ($\boldsymbol{r}$) space and in time (t), and bring to light properties of the turbulent flows which can not be highlighted by conventional single-point budgets or spectra.

Figure 1 is a typical AGKE result for a statistically stationary turbulent channel flow. As in such flow the only statistically non-homogeneous direction is the wall-normal one, the AGKE terms are defined in the (r_x, r_y, r_z, Y) four-dimensional space; x, y and z denote the streamwise, wall-normal and spanwise directions. Additionally, the space of wall-normal scales is defined only for $|r_y|/2 < Y$, owing to the finite extension of the channel in the wall-normal direction. Figure 1 shows the source term of $\langle -\delta u \delta v \rangle$, i.e. the r.h.s. of Eq.1: $\xi_{12} = P_{12} + \Pi_{12} + D_{12}$, in the $r_x = 0$ space. Large positive and negative values of ξ_{12} are found to define two distinct regions in the buffer layer, both involving small wall-normal scales r_y. The region with positive ξ_{12} corresponds to intermediate spanwise scales ($10 \le r_z^+ \le 50$), and the other region to very small ones ($r_z^+ \sim 0$). In the buffer layer, except at the scales corresponding to the region of large positive values, ξ_{12} is negative everywhere. On the contrary, at larger Y, ξ_{12} is slightly positive at all scales. The positive and negative peaks of ξ_{12}, respectively placed at $(r_y^+, r_z^+, Y^+) \sim (0, 20, 13)$ and $(r_y^+, r_z^+, Y^+) \sim (19, 0, 12)$, highlight the different scales of maximum contribution; similarly to the budget of $\langle -uv \rangle$, as D_{12} is negligible in the overall four-dimensional space, the positive contribution to ξ_{12} entirely comes from P_{12}, whereas the negative one from Π_{12}.

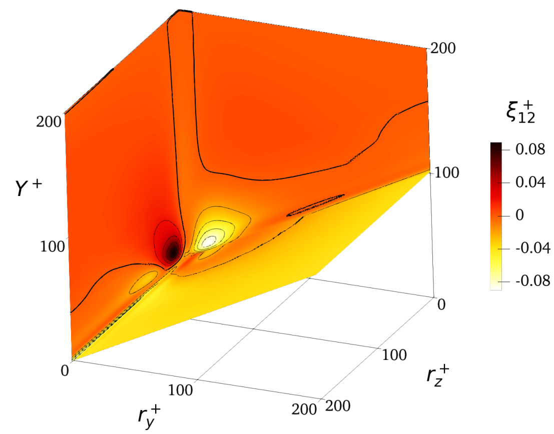

Figure 1: Colour plot of ξ_{12}^+ in the $r_x = 0$ space for a turbulent channel flow. Contour lines increment by 0.02, with zero indicated by a thick line.

Armed with this novel tool, we investigate how a well-known skin-friction drag reduction technique, namely the spanwise-oscillating wall [3], affects this picture. Two (with and without wall oscillations) Direct Numerical Simulations at Constant Power Input (CPI) [2] (carried out at a value of the power-based Re equivalent to $Re_\tau = 200$ for the unforced flow) are carried out, with wall oscillation amplitude and period set at $A^+ = 4.5$ and $T^+ = 125.5$, i.e. near the maximum net energy saving condition [4]. Hereafter, unless otherwise indicated quantities are expressed in power units (see [2] for their definition), whereas the + superscript denotes quantities expressed in actual viscous units.

The comparison of AGKE terms in the controlled and non-controlled cases shows that the oscillating wall modifies production, transport and dissipation of the components of the $\langle \delta u_i \delta u_j \rangle$ tensor. For example, for the $\langle \delta u \delta u \rangle$ component, the oscillating wall shifts the main transfers towards larger wall-distances. This is shown in figure 2. Here the main field lines of fluxes $\boldsymbol{\phi}_{11}$ and ψ_{11}, representative of the transfers of $\langle \delta u \delta u \rangle$ in space and among scales, are shown in the $r_x = r_z = 0$ plane for both the controlled and non-controlled cases. In both cases these field lines originate in the buffer layer at $r_y = 0$. In the first part of their path they follow

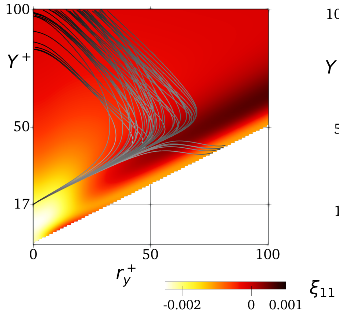

Figure 2: Colour plot of the source term ξ_{11} of $\langle \delta u \delta u \rangle$ in the $r_x = r_z = 0$ space. Gray lines are tangent to the vector of the fluxes. Left: controlled case. Right: non-controlled case.

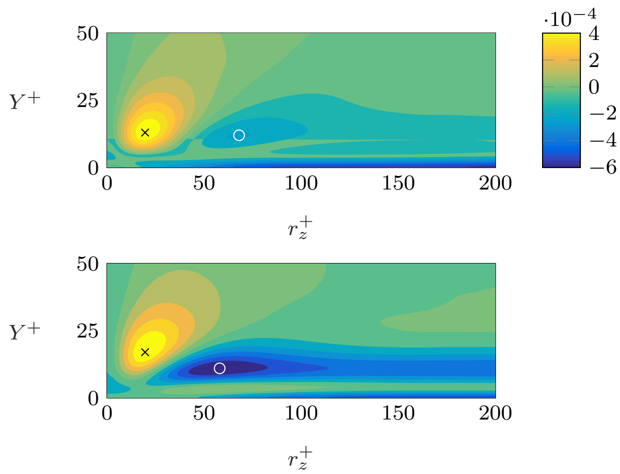

Figure 3: Colour plot of ξ_{12} in the $r_x = r_y = 0$ plane. Top: Non-controlled case. Bottom: Controlled case. The black cross and white circle denote respectively the positions of the positive maximum and negative minimum of ξ_{12} in the plane.

an oblique line described by $Y^+ = r_y^+/2 + K_{11}^+$, parallel to the lower boundary of the domain. This implies a transfer of $\langle \delta u \delta u \rangle$ towards larger wall-distances and towards larger wall-normal scales. Finally, they vanish at larger wall distances at null wall-normal scales, i.e. at the $r_y = 0$ axis, or in correspondence of the wall, i.e. in the lower boundary of the domain; accordingly, at the smallest scales and in the near-wall region $\langle \delta u \delta u \rangle$ is completely dissipated via viscous effects. The effect of the oscillating wall is clearly visible as a shift of these transfers towards larger wall-distances: K_{11}^+ is found to increase from 14 in the non-controlled case, to 17. Interestingly, such changes are not evident for the $\langle \delta v \delta v \rangle$ component: $K_{22}^+ = 40$ in both the controlled and non-controlled cases.

On the contrary, in the off-diagonal component $\langle -\delta u \delta v \rangle$ the oscillating wall changes the wall-normal location and spanwise scale of the maximum production ($P_{12,m}$) and those of the minimum pressure strain ($\Pi_{12,m}$), the main sink contributor. The latter is moved slightly closer to the wall, whereas the former away from; both occur at smaller r_z. This is shown in figure 3 where the source term ξ_{12}, for both the controlled and non-controlled cases, is shown in the $r_x = r_y = 0$ plane, and the positions of its maximum and minimum shown with symbols. The positive peak of ξ_{12} shifts towards larger Y and slightly smaller r_z together with $P_{12,m}$, whereas its relative minimum in this plane shifts towards smaller Y and smaller r_z, together with $\Pi_{12,m}$. The increased offset between the wall-normal positions of $P_{12,m}$ and $\Pi_{12,m}$ results in a larger sink for $\langle -\delta u \delta v \rangle$ in the buffer layer at $r_z^+ > 40$ and $Y^+ \in (7, 20)$, and in a more intense source at slightly larger wall distances, in a region characterized by $r_z^+ > 150$ and $Y^+ \in (25, 50)$.

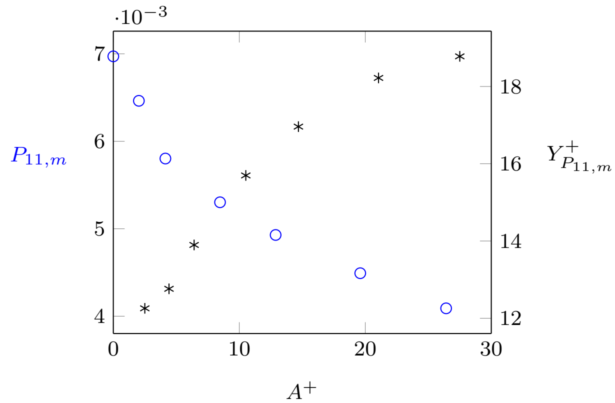

Figure 4: Dependence of the maximum of the production of $\langle \delta u \delta u \rangle$ ($P_{11,m}$) on the amplitude of the oscillating wall (A). Blue circles: intensity (expressed in power units, left axis) versus A^+. Black asterisks: wall-normal position (expressed in actual wall units, right axis) versus A^+.

The most important changes in the AGKE statistics are then studied as a function on the amplitude of the oscillating wall (hence, indirectly, of the amount of drag reduction) in a second phase of the study. Six additional (smaller) DNSs are conducted where the amplitude of the oscillations is varied up to $A^+ = 30$. The analysis highlights several interesting trends. As an example, figure 4 shows how the maximum of the production of $\langle \delta u \delta u \rangle$ ($P_{11,m}$) and its position change with A. The value $P_{11,m}$ of the maximum is found to decrease with A^+. On the contrary, its wall-normal position $Y^+_{P_{11,m}}$ increases significantly with A^+ from $Y^+ \sim 12$ to $Y^+ \sim 19$, seemingly approaching an asymptotic value.

At the conference, the most important changes induced by flow control on the energy fluxes will be addressed, with a view to isolate the key mechanism behind skin-friction drag reduction.

REFERENCES

[1] D. Gatti, A. Chiarini, A. Cimarelli, and M. Quadrio. Production, transport and dissipation of turbulent stresses across scales and space. In *International Turbulence Initiative, Bertinoro (I), Sept. 5-7 2018*, 2018.

[2] Y. Hasegawa, M. Quadrio, and B. Frohnapfel. Numerical simulation of turbulent duct flows at constant power input. *J. Fluid Mech.*, 750:191–209, 2014.

[3] W.J. Jung, N. Mangiavacchi, and R. Akhavan. Suppression of turbulence in wall-bounded flows by high-frequency spanwise oscillations. *Phys. Fluids A*, 4 (8):1605–1607, 1992.

[4] M. Quadrio and P. Ricco. Critical assessment of turbulent drag reduction through spanwise wall oscillation. *J. Fluid Mech.*, 521:251–271, 2004.